

PREPARED FOR SUBMISSION TO JHEP

Probing Bottom-flavored Scalar Dark Matters at Loop Level

Wei Chao,^a Jian-guo Jiang,^a Min Su^a

^a*Center for advanced quantum studies, and Department of Physics, Beijing Normal University, Beijing 100875, China*

E-mail: chaowei@bnu.edu.cn, jgjiang@mail.bnu.edu.cn,
sumin@mail.bnu.edu.cn

ABSTRACT: In this paper we consider loop corrections to the spin-independent WIMP-nucleon scattering cross section in bottom-quark flavored scalar-type dark matter models. We focus on two scenarios: (a) a complex scalar dark matter with a scalar particle as the mediator; and (b) a real scalar dark matter with a vector boson as the mediator. In both scenarios, the direct detection cross sections are either spin-dependent or kinematically forbidden at the tree-level. Corrections induced by the WIMP-gluon effective operator, scalar-type WIMP-quark effective operator, and the twist-2 effective operator are calculated. Numerical results show that loop induced spin-independent WIMP-nucleon scattering cross sections are quite considerable in both scenarios.

Contents

1	Introduction	1
2	Complex scalar DM with spin-0 mediator	3
2.1	Relic density	3
2.1.1	The $m_\varphi < m_\Phi$ scenario	4
2.1.2	The $m_\varphi > m_\Phi$ scenario	4
2.2	Direct detection	5
2.2.1	Effective operator at the next-to-leading order	6
2.2.2	Effects from RGE running and Threshold Matching	7
2.2.3	Scattering cross section	8
3	Real scalar DM with spin-1 mediator	9
3.1	Relic density	10
3.1.1	The $m_{\rho,\eta} < m_{Z'}$ scenario	10
3.1.2	The $m_{\rho,\eta} > m_{Z'}$ scenario	11
3.2	Direct detection	11
3.2.1	Effective operators at loop level	11
4	Numerical results	12
5	Summary	15
A	Annihilation cross sections	16
B	Loop functions	17
C	Nucleon form factors	18

1 Introduction

Various astrophysical observations have confirmed the existence of cold dark matter (DM) [1]. However, what is DM made by and how it couples to the Standard Model (SM) particles still elude us. During the past decades many DM candidates with masses ranging from 10^{-22} eV to 10^{55} GeV have been proposed, of which the weakly interacting massive particles (WIMPs) [2–7] are most promising as they can naturally explain the observed relic density with their masses at the electroweak scale and their interactions as weak as the weak nuclear force.

There are many experiments [8–10] on the Earth designed for probing WIMPs, which can be classified into two categories: the direct detection experiment and the indirect detection experiment. Direct detection experiments measure the nuclear (or the electron)

recoil energy induced by the elastic scattering of WIMPs with nucleon (electron) in underground laboratories. Indirect detection experiments detect the flux of secondary cosmic rays injected by the WIMP annihilations or decays. These two methods are potentially complimentary to each other in testing a WIMP model.

Theoretically, it will be a good strategy to investigate the direct detection signal of a WIMP model that may have non-trivial signals in indirect detection experiments. The AMS-02 collaboration [11] has identified an excess of cosmic-ray antiprotons, which can be explained by the DM annihilation into $b\bar{b}$ with a reduced cross section of $(0.8 \sim 5.2) \times 10^{-26} \text{ cm}^3/\text{s}$ for a DM mass around (64, 88) GeV [12]. Besides, there is an excess of GeV-scale gamma-rays [13–18] observed from the region surrounding the Galactic Center. The spectral shape, morphology and intensity of the excess can also be explained by the annihilation of DM into $b\bar{b}$ with the mass in the range of (40, 70) GeV [19]. Motivated by the fact that the bottom-quark flavored DM models may have non-trivial signals in indirect detection experiments, we study signals of these models in direct detection experiments. It should be noted that the antiproton and GeV gamma ray excesses can also be interpreted by astrophysical sources, and we are not trying to explain these excesses by a bottom-flavored DM model. Instead, our purpose is to provide loop-level analytical result of DM-nucleon scattering cross section that may help to identify a bottom-quark flavored DM in future combined searches of direct and indirect detection experiments.

Due to the technological innovations and advances, the precision and detecting efficiency of direct detection experiments have been greatly improved. For WIMP models, whose scattering cross section with nucleon is spin-independent at the tree-level, the existing experimental accuracy is already able to detect their sensitive parameter space. In this paper, we will focus on two interesting scenarios: (A) a complex scalar DM with a scalar particle as the mediator and (B) a real scalar DM with a spin-1 vector boson as the mediator. In both scenarios, the DM-nucleon cross section is either spin-dependent or kinematically forbidden at the tree-level. As a result, loop corrections [20–35] turn to be the dominant contribution to the spin-independent DM-nucleon cross section. Since the exclusion limit given by direct detections will soon reach the so-called neutrino floor [36–41], below which the DM signal is indistinguishable from an irreducible background induced by the coherent elastic neutrino-nuclei scattering, loop-level calculations will be necessary whenever one wants to find out whether or not such a model is detectable using the current direct detection techniques. Following Refs. [42, 43], we calculate Wilson coefficients of the scalar-type and twist-2 DM-bottom-quark effective operators which arise from the box and triangle diagrams, as well as Wilson coefficient of DM-gluon effective operator [44, 45] which arises at the two-loop level. After accounting for constraints of the observed relic abundance, we find that

- Loop corrections are significant in the scenario A, and most of the parameter spaces of interest to this model can be tested using current direct detection techniques, as shown in the left-panel of the Fig. 10.
- For scenario B, loop effects are relatively small and the DM-nucleon scattering cross section lies above the neutrino floor only in the low DM mass regime, as shown in the

right-panel of the Fig. 10.

It should be mentioned that our analytical results can be directly applied to study the parameter space of interest in future indirect detection experiments.

The remaining of this paper is organized as follows: In section II we calculate the corrections to the DM-nucleon cross section in the scenario A. Section III is devoted to study the direct detection cross section of the scenario B. Numerical results are given in the section IV and the last part is conclusion. The thermal average of the reduced annihilation cross sections, loop integrals and nucleon form factors are given in the appendices, A, B and C.

2 Complex scalar DM with spin-0 mediator

Since we are going to calculate the DM-nucleon scattering cross section at the loop level, a description of DM interactions in the effective field theory approach does not apply. Throughout this paper we consider the direct detection signals of a scalar dark matter, whose interactions take a general form: $\mathcal{L} \supset \overline{\text{DM}} \text{DM Med} + \overline{\text{SM}} \text{SM Med}$, with Med stands for the mediator particle. The Lagrangian of a complex scalar dark matter φ , that couples to the bottom quark via a spin-0 mediator Φ , can be written as

$$-\mathcal{L} \sim \frac{1}{2} \lambda \varphi^\dagger \varphi \Phi^2 + \Lambda \varphi^\dagger \varphi \Phi + f_S \Phi \bar{b} b + f_P \Phi \bar{b} i \gamma_5 b + \text{h.c.} \quad (2.1)$$

where Λ is the coupling with mass dimension. Λ and λ are taken as free parameters, actually they might be correlated with each other via a Higgs mechanism, i.e., $\Lambda = \lambda v_\Phi$ with v_Φ the vacuum expectation value of the Φ . Eq. (2.1) is invariant under a Z_2 discrete flavor symmetry $\varphi \leftrightarrow -\varphi$, which stabilizes the φ as a DM candidate. If there is another Z_2 symmetry for Φ , i.e., $\Phi \rightarrow -\Phi$, then the term $\Lambda \varphi^\dagger \varphi \Phi + \text{h.c.}$ will be forbidden. The Yukawa interactions in Eq. (2.1) may come from integrating out a new vector-like heavy fermion, ψ , which couples to the third generation quark doublet as well as the right-handed bottom quark, $\tilde{y}_b \overline{Q}_L^3 H \psi_R + \zeta \overline{\psi}_L \Phi b_R + \text{h.c.}$, where H is the SM Higgs doublet, \tilde{y}_b and ζ are Yukawa couplings. Apparently there is a rephrasing invariant term in the Lagrangian, $\arg(y_b \tilde{y}_b^* \zeta^* M_\psi)$, which can lead to the CP violation. In this paper, we will only focus on the pseudo-scalar interaction (only $f_P \neq 0$), as the scalar-type interaction will result in spin-independent scattering cross section at the leading order, which is already suppressed by the exclusion limits put by various dark matter direct detection experiments.

2.1 Relic density

The dark matter number density n , is governed by the Boltzmann equation [46]:

$$\dot{n} + 3Hn = -\langle \sigma v_{\text{Møller}} \rangle (n^2 - n_{\text{EQ}}^2), \quad (2.2)$$

where H is the Hubble constant, $\sigma v_{\text{Møller}}$ is the total annihilation cross section multiplied by the Møller velocity, $v_{\text{Møller}} = (|v_1 - v_2|^2 - |v_1 \times v_2|^2)^{1/2}$, brackets denote thermal average and n_{EQ} is the number density at the thermal equilibrium. It has been shown that $\langle \sigma v_{\text{Møller}} \rangle = \langle \sigma v_{\text{lab}} \rangle = 1/2[1 + K_1^2(x)/K_2^2(x)]\langle \sigma v_{\text{cm}} \rangle$ [46], where $x = m/T$, K_i is the modified Bessel functions of order i .

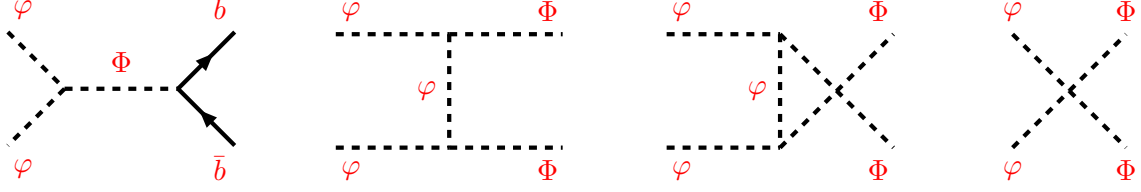


Figure 1: Annihilation channels of complex scalar dark matter φ with a spin-0 mediator Φ . All Feynman diagrams are drawn with the help of TikZ-Feynman [47].

2.1.1 The $m_\varphi < m_\Phi$ scenario

In the mass regime $m_\varphi < m_\Phi$, the annihilation channel $\varphi\varphi \rightarrow \Phi\Phi$ is kinematically forbidden and there is only one annihilation channel $\varphi\varphi \rightarrow \bar{b}b$ which is given in the most left plot of the Fig. 1. The annihilation cross section can be written as

$$\sigma(\varphi\varphi \rightarrow \bar{b}b) = \frac{1}{8\pi} \sqrt{\frac{s - 4m_b^2}{s - 4m_\varphi^2}} \frac{\Lambda^2 f_P^2}{(s - m_\Phi^2)^2 + m_\Phi^2 \Gamma_\Phi^2}, \quad (2.3)$$

where Γ_Φ is the decay rate of Φ ,

$$\Gamma_\Phi = \frac{1}{8\pi} f_P^2 \sqrt{m_\Phi^2 - 4m_b^2} + \Theta(m_\Phi - 2m_\varphi) \frac{1}{16\pi} \frac{\Lambda^2}{m_\Phi^2} \sqrt{m_\Phi^2 - 4m_\varphi^2}, \quad (2.4)$$

with $\Theta(x)$ the unit step function. Analytically one can approximate the thermal average $\langle\sigma v\rangle$ with the non-relativistic expansion $\langle\sigma v\rangle = a + b\langle v^2\rangle$ in the laboratory frame, where a and b are given in the Appendix A.

The present relic density of the DM is simply given by $\rho_\chi = m_\chi n_\chi = m_\chi s_0 Y_\infty$, where s_0 is the present entropy density. The relic density can finally be expressed in terms of the critical density [7]

$$\Omega h^2 \approx 2 \times \frac{1.07 \times 10^9 \text{GeV}^{-1} x_F}{M_{pl} \sqrt{g_*} (a + 3b/x_F)}, \quad (2.5)$$

where M_{pl} is the Planck mass, a and b , expressed in GeV^{-2} , are the s -wave and the p -wave parts of the reduced annihilation cross section and g_* is the effective degrees of freedom at the freeze-out temperature T_F , $x_F = M/T_F$, which is of the order $\mathcal{O}(22)$, the factor 2 on the right-handed side accounts for the fact that the dark matter is a complex scalar.

2.1.2 The $m_\varphi > m_\Phi$ scenario

In the mass regime $m_\varphi > m_\Phi$, the annihilation channel $\varphi\varphi \rightarrow \Phi\Phi$, as shown in the remaining plots of the Fig. 1, is kinematically allowed. The annihilation cross section in the center-of-mass framework is

$$\sigma(\varphi\varphi \rightarrow \Phi\Phi) = \frac{1}{32\pi s} \sqrt{\frac{s - 4m_\Phi^2}{s - 4m_\varphi^2}} \left[\frac{2\Lambda^4}{A^2 - B^2} + \frac{2\Lambda^2(\Lambda^2 - 2A\lambda)}{AB} \tanh^{-1}\left(\frac{B}{A}\right) + \lambda^2 \right] \quad (2.6)$$

where $A = s/2 - m_\Phi^2$ and $B = 1/2\sqrt{(s - 4m_\varphi^2)(s - 4m_\Phi^2)}$. One may get the thermal average of the reduced annihilation cross section with the help of Eq. (2.6), and expressions of s -wave and p -wave contributions are given in Appendix A, with the help of which one may estimate the relic abundance of φ .

2.2 Direct detection

The dark matter direct detection experiments aim to observe phonon, light or ionization generated by the recoiled nuclei arising from the scattering of dark matter off the nuclei. The WIMP event rate can be written as [48]

$$\frac{dR}{dE_R} = MT \times \frac{\rho_\chi \sigma_n^0 A^2}{2m_\chi \mu_n^2} F^2(E_R) \int_{v_{\min}} \frac{f(\vec{v})}{v} d^3v \quad (2.7)$$

where M is the target mass, T is the exposure time, ρ_χ is the DM density in the local halo, μ_n is the DM-nucleon reduced mass, σ_n^0 is the DM-nucleon cross section, A is the atomic number, $F(E_R)$ is the nuclear form factor and we use the Helm form factor [49], $f(\vec{v})$ is the DM velocity distribution, v_{\min} depends on E_R : $v_{\min} = \sqrt{m_T E_R / 2\mu_T^2}$ with μ_T the DM-nucleus reduced mass.

There are two ways measuring the local DM density ρ_χ [50]: local measures that use the vertical kinematics of stars near the Sun, called tracers, and global measures that extrapolate ρ_χ from the rotation curve. Its value is given with a large uncertainty as $\rho_\chi = (0.2 - 0.6)$ GeV. There is no way to measure $f(\vec{v})$ directly, it is usually assumed to be the Maxwell-Boltzmann distribution function in the galactic center coordinate. The velocity integral in eq. (2.7) can be analytically written as [51]

$$\int_{v_{\min}} \frac{f(\vec{v})}{v} d^3v = \frac{1}{2v_0 \eta_E} [\text{erf}(\eta_+) - \text{erf}(\eta_-)] - \frac{1}{\pi v_0 \eta_E} (\eta_+ - \eta_-) e^{-\eta_{\text{esc}}^2} \quad (2.8)$$

where v_0 is the speed of the Local Standard of Rest, $\eta_E = v_E/v_0$ with v_E the Earth velocity with respect to the galactic center, $\eta_{\text{esc}} = v_{\text{esc}}/v_0$ with v_{esc} the escape velocity of DM from our galaxy, $\eta_\pm = \min(v_{\min}/v_0 \pm \eta_E, v_{\text{esc}}/v_0)$. We take $v_0 = 220$ km/s, $v_{\text{esc}} = 544$ km/s and $\vec{v}_E = \vec{v}_\odot + \vec{v}_\oplus \approx \vec{v}_\odot = 232$ km/s, where \vec{v}_\odot and \vec{v}_\oplus are the velocity of the Sun with respect to the Galaxy as well as the Earth rotational velocity, respectively.

According to the Eq. (2.7), the non-observation of any DM signal for a concrete DM direct detection experiment with fixed exposure, will generate the exclusion limit on the direct detection cross section in the $m_{\text{DM}} - \sigma_n^0$ plane, so an analytical calculation of σ_n^0 is necessary so as to put constraint on the parameter space of the model. For the complex scalar dark matter φ with spin-0 mediator, the scattering cross section is spin-dependent and the effective operator at the quark level can be written as

$$\mathcal{L}_b \sim -\frac{\Lambda f_P}{m_\Phi^2} \phi^\dagger \phi \bar{b} i \gamma_5 b \quad (2.9)$$

Bottom quark is heavier than the proton and should be integrated out of an effective theory describing physics at nuclear scale. Integrating out the bottom quark, one has loop induced

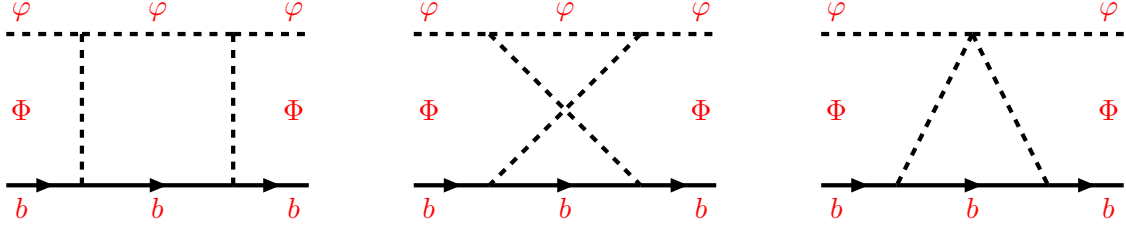


Figure 2: Box and triangle diagrams for the effective WIMP-bottom quark interactions with spin-0 mediator.

coupling with gluon [52],

$$\mathcal{L}_g \sim \frac{\alpha_s}{8\pi} \frac{\Lambda f_P}{m_b m_\Phi^2} \phi^\dagger \phi G_{\mu\nu}^a \tilde{G}^{a\mu\nu} \quad (2.10)$$

where $\tilde{G}_{\mu\nu}^a = \varepsilon_{\mu\nu\rho\sigma} G_{\rho\sigma}^a$ with the convention $\varepsilon_{0123} = 1$. Now one can write down the effective Lagrangian at the nucleon level

$$\mathcal{L}_N \sim m_N \bar{m} \left(\sum_{q=u,d,s} \frac{\Delta_q^N}{m_q} \right) \frac{\Lambda f_P}{m_b m_\Phi^2} \phi^\dagger \phi \bar{N} i \gamma_5 N \quad (2.11)$$

where $\bar{m} = (1/m_u + 1/m_d + 1/m_s)^{-1}$, $\Delta_u^N = 0.84$, $\Delta_d^N = -0.43$ and $\Delta_s^N = -0.09$ [53]. The spin-dependent DM-nuclei cross section can be written as

$$\sigma_{SD} = \frac{1}{32\pi} \frac{q^2}{(m_\phi + m_N)^2} \left[m_N \bar{m} \left(\sum_{q=u,d,s} \frac{\Delta_q^N}{m_q} \right) \frac{\Lambda f_P}{m_b m_\Phi^2} \right]^2 \quad (2.12)$$

where q is the momentum transfer. Apparently this cross section is kinematically suppressed by the factor q^2 . One needs to calculate the spin-independent cross section at the next-to-leading order to probe the model.

2.2.1 Effective operator at the next-to-leading order

To derive the loop corrections to the spin-independent DM-nucleon scattering cross section, we first need to calculate the Wilson coefficients of DM-quark and DM-gluon effective operators. Following Refs. [42, 43], relevant effective operators take the form:

$$\mathcal{L}_{\text{eff}} \sim C^{\text{twist2}} \phi^\dagger i \partial^\mu i \partial^\nu \phi \mathcal{O}_{\mu\nu}^b + C^{\text{scalar}} \phi^\dagger \phi m_b \bar{b} b + C^{\text{gluon}} \phi^\dagger \phi \frac{\alpha_s}{12\pi} G_{\mu\nu}^a G^{a\mu\nu} \quad (2.13)$$

where $\mathcal{O}_{\mu\nu}^b$ is the twist-2 operator defined by

$$\mathcal{O}_{\mu\nu}^b = \frac{i}{2} \bar{b} (\partial_\mu \gamma_\nu + \partial_\nu \gamma_\mu - \frac{1}{2} g_{\mu\nu} \not{\partial}) b. \quad (2.14)$$

Wilson coefficients for scalar-type DM-bottom quark operator and the twist-2 operator, C^{scalar} and C^{twist2} , are generated by the box and triangle diagrams in Fig. 2. The two-loop

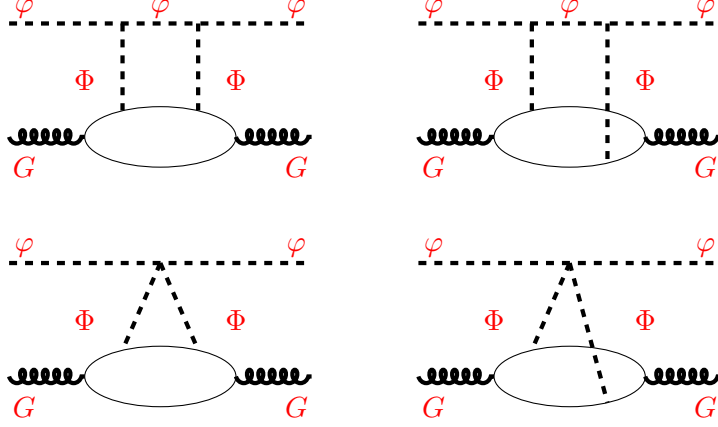


Figure 3: Two-loop diagrams for effective WIMP-gluon interactions with spin-0 mediator.

diagrams in Fig. 3 with only bottom quark running in the loop contribute to the scalar-type DM-gluon operator with the Wilson coefficient C^{gluon} .

Box and triangle diagrams are calculated in the zero-momentum transfer limit for simplification. We further expand the integral by the bottom quark momentum and only keep the leading term [31] in the calculation. Then the Wilson coefficients C^{scalar} and C^{twist2} can be obtained by reading out the DM-quark effective operators. For the DM-gluon coefficient C^{gluon} , one needs to calculate the amplitude of two-loop diagrams and find the effective operator $\varphi^\dagger \varphi G_{\mu\nu}^a G^{a\mu\nu}$. It should be noted that high twist DM-gluon effective operator, whose impacts to the DM-nuclei scattering cross section is sub-dominant, is neglected in this paper. We use the Fock-Schwinger gauge [54, 55] for the gluon field, which makes the calculation transparent. Then the two-loop amplitude can be expressed using the two-point function of scalar field in the gluon background field. From this amplitude one can obtain the Wilson coefficient C^{gluon} . All relevant Wilson coefficients are summarized as follows:

$$C^{\text{twist2}} = -\frac{4(f_p \Lambda)^2}{16\pi^2} Z_{11}(m_\varphi^2, m_\varphi^2, m_\Phi^2) \quad (2.15)$$

$$C^{\text{scalar}} = \frac{1}{16\pi^2} \left\{ (f_p \Lambda)^2 [-4Z_{00}(m_\varphi^2, m_\varphi^2, m_\Phi^2) - m_\varphi^2 Z_{11}(m_\varphi^2, m_\varphi^2, m_\Phi^2)] + \lambda f_p^2 C_2(m_b^2, m_\Phi^2, m_b^2) \right\} \quad (2.16)$$

$$C^{\text{gluon}} = \frac{1}{32\pi^2} \left[(f_P \Lambda)^2 \frac{\partial F_1(m_\Phi^2)}{\partial m_\Phi^2} + \lambda f_P^2 \frac{\partial F_2(m_\Phi^2)}{\partial m_\Phi^2} \right] \quad (2.17)$$

where the loop functions Z_{11} , Z_{00} , $F_1(m_\Phi^2)$ and $F_2(m_\Phi^2)$ are given in the Appendix B. In our numerical calculations, we use Package-X [56, 57] to compute the above loop functions.

2.2.2 Effects from RGE running and Threshold Matching

The effective operators and Wilson coefficients obtained above are defined at the electroweak scale $\mu = M_Z$ and need to evolve to the hadron scale $\mu_{\text{hadron}} \approx 1 \text{ GeV}$. They evolve by means of renormalization group equations (RGEs). As shown in the Eq. (2.13), one needs to

account the running of scalar-type operators and a twist-2 operator. The QED contributions to the renormalization group evolution can be neglected taking into account the smallness of the electromagnetic coupling constant. Notice that DM is a QCD and QED singlet, so the RGE evolution is mainly due to the SM fields in the effective operators. The quark mass operator has vanishing anomalous dimension in a mass-independent renormalization scheme like the $\overline{\text{MS}}$ scheme [42],

$$\mu \frac{d}{d\mu} m_q \bar{q}q = 0. \quad (2.18)$$

By differentiating the trace of energy-momentum tensor in QCD, one further has $\mu \frac{d}{d\mu} \left(\frac{\alpha_s}{\pi} GG \right) = 0$, which implies the Wilson coefficients of scalar-type operators are RGE invariant. Finite corrections arise at the bottom quark threshold, $\mu = \mu_b$,

$$C^{\text{gluon}}|_{\mu=\mu_b} \rightarrow C^{\text{gluon}}|_{\mu=\mu_b} - C^{\text{scalar}}|_{\mu=\mu_b}, \quad (2.19)$$

and also there is threshold corrections to α_s [58]. As a result, the effect of the DM-bottom-quark operator appears as an extra contribution to the DM-gluon effective operator.

To evaluate the RGE effect of the twist-2 effective operator in Eq. (2.13), we need to introduce the twist-2 operator of gluon with the Wilson C_g^{twist2} . The relevant RGE is [59]

$$\frac{d}{d \ln \mu} (C_q^{\text{twist2}}, C_g^{\text{twist2}}) = (C_q^{\text{twist2}}, C_g^{\text{twist2}}) \Gamma \quad (2.20)$$

with

$$\Gamma = \frac{\alpha_s}{4\pi} \begin{pmatrix} \frac{16}{3}C_F & 0 & \cdots & 0 & \frac{4}{3} \\ 0 & \frac{16}{3}C_F & 0 & \cdots & \frac{4}{3} \\ \cdots & \cdots & \cdots & \cdots & \cdots \\ \frac{16}{3}C_F & \cdots & \cdots & \frac{16}{3}C_F & \frac{4}{3}N_f \end{pmatrix} \quad (2.21)$$

where $C_F = 4/3$ being the quadratic Casimir invariant and N_f is the number of quark family. Γ is a $(N_f + 1) \times (N_f + 1)$ matrix. Wilson coefficients of twist-2 operators cross thresholds continuously.

2.2.3 Scattering cross section

The spin-independent scattering cross section can then be written as

$$\sigma^{\text{SI}} = \frac{\mu^2}{8\pi} \frac{m_N^2}{m_\varphi^2} \left[\left(C^{\text{scalar}} - C^{\text{gluon}} \right) f_{T_b}^N + \sum_q C_q^{\text{twist2}} \frac{3}{4} m_\varphi^2 (\bar{q}^N + q^N) - \frac{3}{4} C_g^{\text{twist2}} m_\varphi^2 G^N \right]^2, \quad (2.22)$$

where

$$f_{T_b}^N = \frac{2}{27} \left(1 - \sum_{u,d,s} f_{T_q}^N \right) = \frac{2}{27} f_{T_G}^N, \quad (2.23)$$

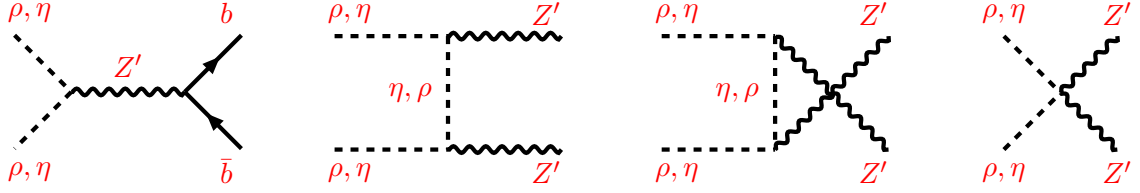


Figure 4: Annihilation channels of real scalar dark matter ρ with a spin-1 mediator Z' .

is the nucleon matrix element of bottom quark, q^N , \bar{q}^N and G^N is the second moment of quarks, antiquarks and gluon in the nucleon, m_N is the nucleon mass and μ is the reduced mass of the WIMP-nucleon system. The numerical values of nucleon form factors are given in the Appendix C. Non-zero twist-2 Wilson coefficients for light quarks and gluon come from the RGE running in the Eq. (2.20).

3 Real scalar DM with spin-1 mediator

In this section we assume a complex scalar φ couples to the SM via a spin-1 mediator Z'_μ , which can be either a new gauge boson for a spontaneously broken $U(1)$ gauge symmetry or a matter field. Here we take Z' as a gauge boson for simplicity. The Lagrangian for the φ can be written as

$$\mathcal{L} \sim (D_\mu \varphi)^\dagger (D^\mu \varphi) + (D_\mu \phi)^\dagger (D^\mu \phi) - V(\varphi, \phi) - \zeta \bar{b} \gamma^\mu b Z'_\mu \quad (3.1)$$

where ϕ is the scalar boson whose vacuum expectation value leads to the spontaneous breaking of the $U(1)$ gauge symmetry as well as the origin of the Z' mass, ζ equals to the new gauge coupling g_V times the hypercharge of the bottom quark, and

$$D_\mu = \partial_\mu - i g_V Z'_\mu. \quad (3.2)$$

The scalar potential can be written as

$$V(\phi, \varphi) = -\mu_\phi^2 \phi^\dagger \phi + \mu_\varphi^2 \varphi^\dagger \varphi + \lambda_\phi (\phi^\dagger \phi)^2 + \lambda_\varphi (\varphi^\dagger \varphi)^2 + \lambda_{\varphi\phi} \varphi^\dagger \varphi \phi^\dagger \phi + \lambda'_{\varphi\phi} (\varphi^2 + h.c.) \phi^\dagger \phi, \quad (3.3)$$

where $\varphi = (\rho + i\eta)/\sqrt{2}$ and $\phi = (v_\phi + \sigma + iG)/\sqrt{2}$. The potential has a Z_2 discrete symmetry, $\varphi \leftrightarrow -\varphi$, which stabilizes φ . Due to the last term in the potential, there might be mass splitting between the CP-even and the CP-odd components of φ ,

$$m_{\rho, \eta}^2 = \mu_\varphi^2 + \frac{1}{2} \lambda_{\varphi\phi} v_\phi^2 \pm \lambda'_{\varphi\phi} v_\phi^2 \quad (3.4)$$

and only the lighter component (here we take it as the CP-even component ρ) can serve as the dark matter candidate, which is quite similar to the case of the inert dark matter in two-Higgs doublet models [60]. η will decay into ρ plus SM particles. We further assume that σ is much heavier than ρ , since the case of scalar portal has already been studied in the

last section and we will not study the σ portal in this case. As a result, ρ mainly annihilate into $\bar{b}b$ and $Z'Z'$ final states, which will be discussed in the following subsection. It should be noted that the SM Higgs is supposed to be decoupled from the hidden Higgs sector for simplicity. A systematic study of the scalar mass spectrum and various constraints from precision measurements for a general Higgs potential is beyond the reach of this paper. We refer the reader to Ref. [61] and references cited therein for details.

As can be seen from the Eq. (3.1), Z' couples to the vector-bilinear of bottom quark. Such an interaction is true in the $U(1)_{B-L}$ [62], $U(1)_{B+L}$ [63] and $U(1)_{B_i-B_3}$ [64] models. Since the main purpose of this paper is to estimate the loop corrections to the direct detection cross section, we will not focus on any specific model. Corrections induced by axial-vector current is similar to the vector current case.

3.1 Relic density

In this subsection we calculate the relic density of scalar DM in the vector-portal. As mentioned above, we are interested in the scenario where η is slightly heavier than ρ . As a result, one needs to include the co-annihilation [65] effect and the DM number density can be written as,

$$n_{\text{DM}} = n_\rho + n_\eta, \quad (3.5)$$

where n_ρ and n_η are number densities of ρ and η respectively.

3.1.1 The $m_{\rho,\eta} < m_{Z'}$ scenario

In the mass regime $m_{\rho,\eta} < m_{Z'}$, the annihilation channel $\rho\rho(\eta\eta) \rightarrow Z'Z'$ is kinematically forbidden and there is only one annihilation channel $\rho\eta \rightarrow \bar{b}b$ which is given in the most left-panel of the Fig. 4. The annihilation cross section can be written as

$$\sigma \approx \frac{\zeta^2 g_V^2}{12\pi s} \frac{(s - 4m_\rho^2)(s + 2m_b^2)}{(s - m_{Z'}^2)^2 + m_{Z'}^2 \Gamma_{Z'}^2} \sqrt{\frac{s - 4m_b^2}{s - 4m_\rho^2}} \quad (3.6)$$

where we have neglected the correction induced by the mass difference, and $\Gamma_{Z'}$ is the decay rate of Z' ,

$$\begin{aligned} \Gamma_{Z'} = & \frac{\zeta^2}{4\pi} \left(1 + \frac{2m_b^2}{m_{Z'}^2} \right) \sqrt{m_{Z'}^2 - 4m_b^2} \\ & + \Theta(m_{Z'} - 2m_\rho) \frac{g_V^2}{16\pi} \left(1 - \frac{4m_\rho^2}{m_{Z'}^2} \right) \sqrt{m_{Z'}^2 - 4m_\rho^2} \end{aligned} \quad (3.7)$$

with $\Theta(x)$ the unit step function. Analytically one can approximate the thermal average $\langle \sigma v \rangle$ with the non-relativistic expansion $\langle \sigma v \rangle = a + b \langle v^2 \rangle$ in the laboratory frame, where a and b are given in the Appendix A.

3.1.2 The $m_{\rho,\eta} > m_{Z'}$ scenario

In the mass regime $m_{\rho,\eta} > m_{Z'}$, the annihilation channel $\rho\rho(\eta\eta) \rightarrow Z'Z'$, as shown in the remaining panels of Fig. 4, is kinematically allowed. The annihilation cross section in the center-of-mass framework is

$$\sigma = \frac{g_V^4}{16\pi s} \left[4 + \frac{(m_{Z'}^2 - 4m_\varphi^2)^2}{A^2 - B^2} + \frac{4s(m_{Z'}^2 - 2m_\varphi^2) + (m_{Z'}^2 - 4m_\varphi^2)^2}{AB} \tanh^{-1} \left(\frac{B}{A} \right) \right] \quad (3.8)$$

where $A = s/2 - m_{Z'}^2$, and $B = 1/2\sqrt{(s - 4m_\varphi^2)(s - 4m_{Z'}^2)}$ with $\varphi = \rho, \eta$. The expressions of s -wave and p -wave contributions are given in the Appendix A, with the help of which one may estimate the relic abundance of DM.

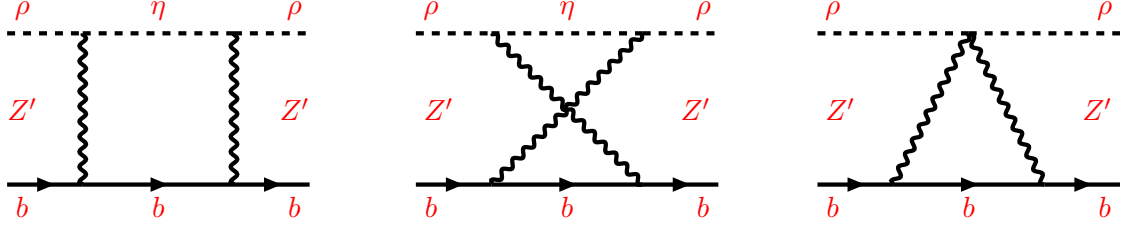


Figure 5: Box and triangle diagrams for the effective WIMP-bottom quark interactions with spin-1 mediator.

3.2 Direct detection

Since DM is non-relativistic, the process $\rho + N \rightarrow \eta + N$ is kinematically forbidden at the tree level. Although the process $\eta + N \rightarrow N + \rho$ is allowed, the number density of η is negligibly small, which leads to null signal in direct detection experiments unless there is a mechanism that can produce η near the Earth. DM-nucleon scatterings arise at the loop level in this scenario.

3.2.1 Effective operators at loop level

The effective DM-quark interactions can be generated at loop-level by box diagrams or the triangle diagram, as shown in the Fig. 5. The DM-gluon interaction is generated at the two-loop level in the Fig. 6. The effective Lagrangian can be written as

$$\mathcal{L}_{\text{eff}} \sim C^{\text{twist}2} \rho i \partial^\mu i \partial^\nu \rho \mathcal{O}_{\mu\nu}^b + C^{\text{scalar}} \rho^2 m_b \bar{b} b + C^{\text{gluon}} \rho^2 \frac{\alpha_s}{12\pi} G_{\mu\nu}^a G^{a\mu\nu}. \quad (3.9)$$

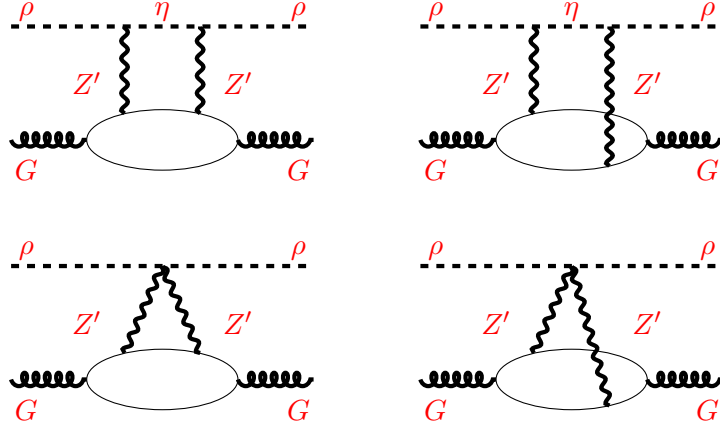


Figure 6: Two-loop diagrams for effective WIMP-gluon interactions for spin-1 mediator.

Wilson coefficients for effective DM-quark operators are given as

$$C^{\text{twist2}} = \frac{(\zeta g_V)^2}{16\pi^2} \left[16X_1(m_\varphi^2, m_\varphi^2, 0, m_{Z'}^2) - 16m_\varphi^2 Z_{11}(m_\varphi^2, m_\varphi^2, m_{Z'}^2) - 32Z_{00}(m_\varphi^2, m_\varphi^2, m_{Z'}^2) \right] \quad (3.10)$$

$$C^{\text{scalar}} = \frac{(\zeta g_V)^2}{16\pi^2} \left\{ \frac{1}{4} m_\varphi^2 \left[16X_1(m_\varphi^2, m_\varphi^2, 0, m_{Z'}^2) - 16m_\varphi^2 Z_{11}(m_\varphi^2, m_\varphi^2, m_{Z'}^2) - 32Z_{00}(m_\varphi^2, m_\varphi^2, m_{Z'}^2) \right] + \left[16m_\varphi^2 Z_{00}(m_\varphi^2, m_\varphi^2, m_{Z'}^2) + 2C_2(m_b^2, m_{Z'}^2, m_b^2) - 2C_0(m_b^2, m_{Z'}^2, m_b^2) \right] \right\} \quad (3.11)$$

To calculate the Wilson coefficient for the DM-gluon interaction, one needs the two-point function of Z' in the gluon background field, which can be written as

$$i\Pi_{Z'Z'}^{\alpha\beta}(q^2) = -\frac{i\zeta^2\alpha_s}{12\pi} G_{\mu\nu}^a G^{a\mu\nu} \left(-\frac{g^{\alpha\beta}}{q^2} + \frac{q^\alpha q^\beta}{q^4} \right) \quad (3.12)$$

Then the Wilson coefficient of DM-gluon operator is

$$C^{\text{gluon}} = \frac{(\zeta g_V)^2}{16\pi^2} \left\{ 4m_\varphi^2 \left[-X_2(m_\varphi^2, m_\varphi^2, 0, m_{Z'}^2) + Z_{00}(m_\varphi^2, m_\varphi^2, m_{Z'}^2) + m_\varphi^2 Z_{11}(m_\varphi^2, m_\varphi^2, m_{Z'}^2) \right] + 6C_0(0, m_{Z'}^2, 0) \right\}. \quad (3.13)$$

Note that the RGE running of Wilson coefficients are the same as those discussed in the last section. The DM-nucleon cross section is the same as Eq. (2.22) up to replacements of Wilson coefficients.

4 Numerical results

In this section we present the numerical results for our models. We start by determining the couplings using the measured DM relic density $\Omega h^2 = 0.1198$. For the spin-0 mediator

case, we show in the left panel of the Fig. 7 the coupling Λ as the function of dark matter mass m_φ , by setting $f_P = 1.5$, $\lambda = 0.1$ and $m_\Phi = 100$ GeV. The first dip appears at $m_\varphi \sim m_\Phi/2$, where the annihilation $\varphi^\dagger\varphi \rightarrow \bar{b}b$ is resonantly enhanced. The second dip at $m_\varphi \sim m_\Phi$ is due to the opening of the annihilation channel $\varphi^\dagger\varphi \rightarrow \Phi\Phi$. The similar procedure can be applied to the spin-1 mediator case, for which the new gauge coupling g_V as the function of dark matter mass is shown in the right panel of the Fig. 7, by setting $\zeta = g_V$ and $m_{Z'} = 100$ GeV. It should be noted that there is only one viable annihilation channel $\varphi^\dagger\varphi \rightarrow \bar{b}b$ for $m_\varphi < m_{Z'}$ which is p -wave suppressed, while $\varphi^\dagger\varphi \rightarrow Z'Z'$ has both s -wave and p -wave components, so the second dip at $m_\varphi = m_{Z'}$ is significant.

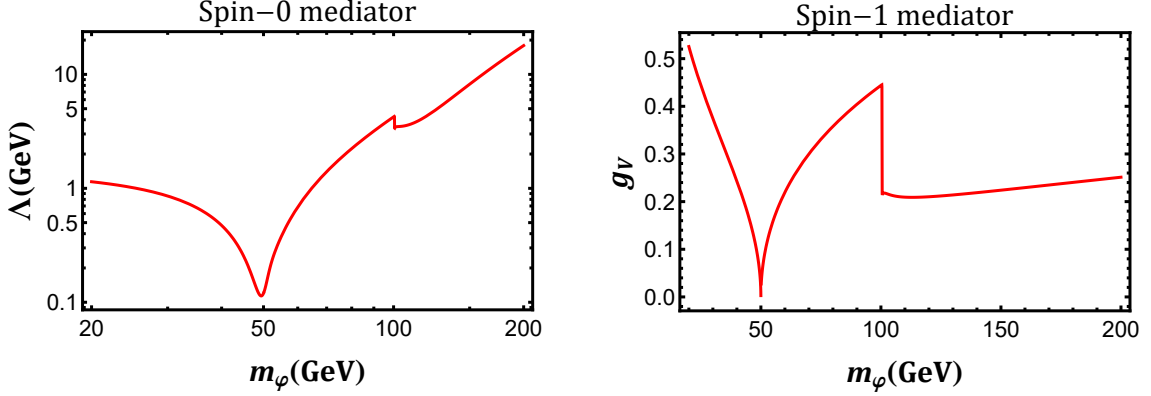


Figure 7: Left panel: Coupling Λ as the function of the DM mass m_φ by setting $f_P = 1.5$, $\lambda = 0.1$ and $m_\Phi = 100$ GeV. Right panel: New gauge coupling g_V as the function of m_φ by setting $\zeta = g_V$ and $m_{Z'} = 100$ GeV. Both are constrained by the observed dark matter relic density $\Omega h^2 = 0.1198$.

We show in the left panel of Fig. 8 contour plot of Λ in the $m_\varphi - m_\Phi$ plane, by setting $f_P = 1.5$, $\lambda = 0.1$. The red, green and blue dashed lines correspond to $\Lambda = 0.5, 1, 2$, respectively. There are two gray solid lines in the plot, the lighter one for $m_\Phi = 2m_\varphi$ and the darker one for $m_\Phi = m_\varphi$, which divide the $m_\varphi - m_\Phi$ plane into three regions, I, II and III. For the region I and II, there is only one annihilation channel $\varphi^\dagger\varphi \rightarrow \bar{b}b$ allowed, where the only difference is that the decay channel $\Phi \rightarrow \varphi^\dagger\varphi$ is allowed in the region I, but forbidden in the region II. In the region III, the new channel $\varphi^\dagger\varphi \rightarrow \Phi\Phi$ is allowed. The contours for g_V are shown in the right panel of Fig. 8, where the red, green and blue dashed lines correspond to $g_V = 0.5, 1, 2$ respectively. Notice that $\mathcal{O}(g_V) \sim 1$ for $m_{Z'} \sim m_\varphi \sim 200$ GeV.

We show in the Fig. 9 Wilson coefficients as the function of the dark matter mass m_φ . The plot for the spin-0 mediator case is given in the left-panel, by setting $f_P = 1.5$, $\zeta = 0.1$, $\Lambda = 0.5$ and $m_\Phi = 100$ GeV. As can be seen, the Wilson coefficient for the gluon-DM operator is the largest, which is of the order $\mathcal{O}(10^{-7})$. The Wilson coefficient for quark-DM operator is smaller than that of the gluon-DM operator by a factor of $\mathcal{O}(5)$. The plot in the right panel shows the Wilson coefficients for spin-1 mediator case by setting $\zeta = g_V = 0.5$. Notice that the Wilson coefficients of the gluon-DM and the scalar-type

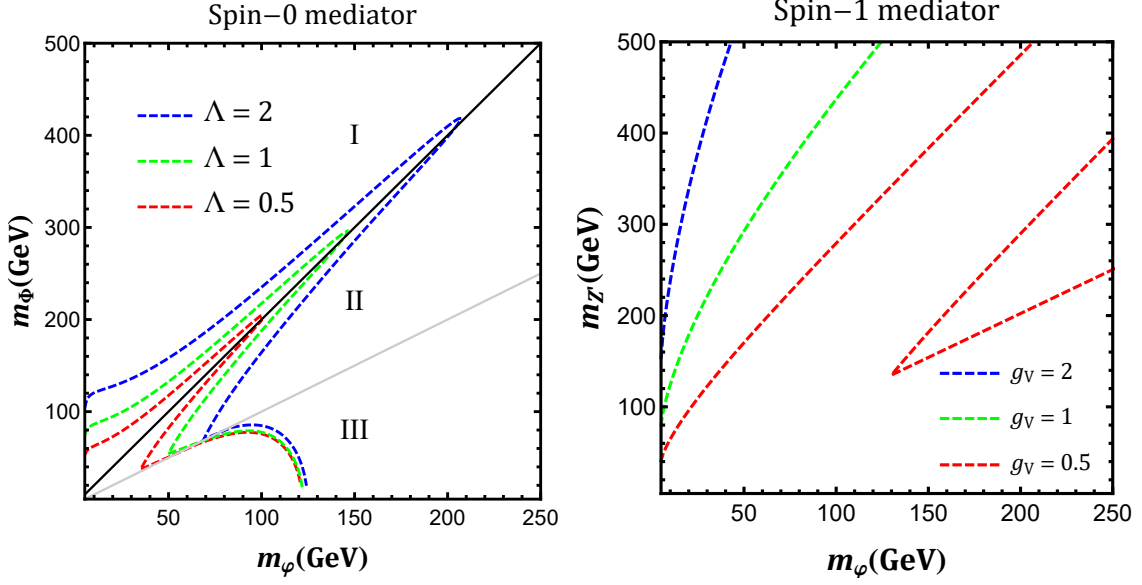


Figure 8: Left panel: Contours of Λ in the $m_\phi - m_\Phi$ plane by setting $f_P = 1.5$, $\lambda = 0.1$. Right panel: Contours of g_V in the $m_\phi - m_{Z'}$ plane by setting $\zeta = g_V$.

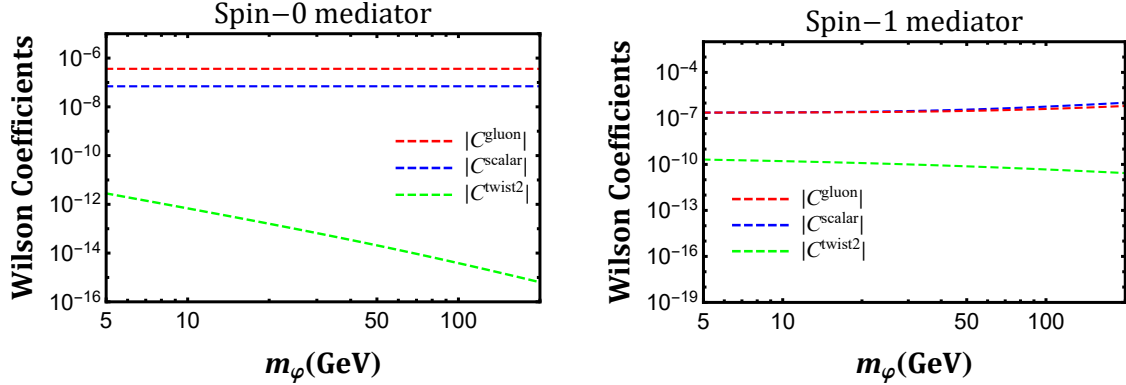


Figure 9: Wilson coefficients as the function of the dark matter mass m_ϕ by setting $f_P = 1.5$, $\lambda = 0.1$, $\Lambda = 0.5$, $m_\Phi = 100$ GeV for spin-0 mediator (left-panel) and $\zeta = g_V = 0.5$, $m_{Z'} = 100$ GeV for spin-1 mediator (right-panel).

quark-DM operators are almost the same.

Finally, we consider the spin-independent DM-nucleon elastic scattering cross section. As an illustration, we show in the Fig. 10 the direct detection cross section as the function of the dark matter mass m_ϕ . The spin-0 mediator case is shown in the left-panel by setting $f_P = 1.5$, $\lambda = 0.1$ and $m_\Phi = 100$ GeV. The green dashed and black dashed lines are exclusion limits put by XENON1T [66] and PandaX-II [67] experiments, separately. There is a wide range of mass (9 – 80) GeV that can be detected with the help of current direct detection techniques. The plot in the right-panel corresponds to the spin-1 mediator case by setting $\zeta = g_V$ and $M_{Z'} = 100$ GeV, for which there is only a narrow mass range

(15 – 23) GeV lying above the neutrino floor. The reason leading to a small cross section is that the contributions from quark-DM and gluon-DM operators cancels with each other as can be seen from the right-panel of the Fig. 9.

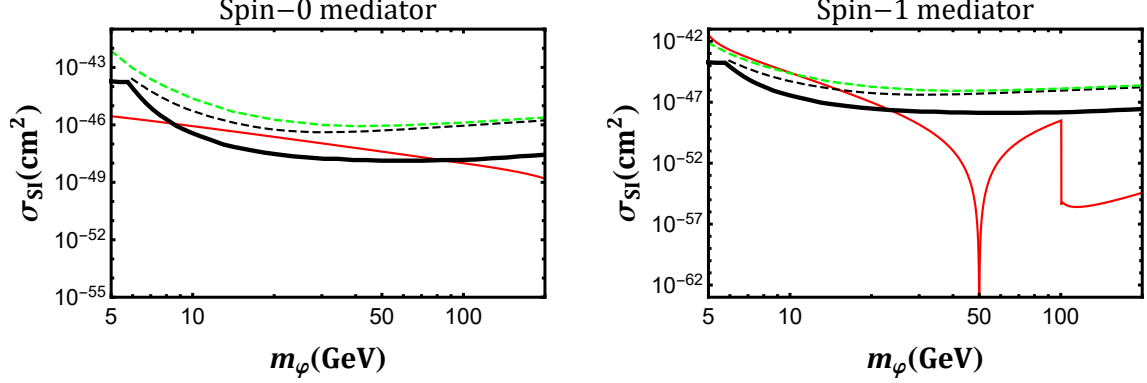


Figure 10: Spin-independent DM-nucleon cross section as the function of the dark matter mass m_φ by setting $f_P = 1.5$, $\lambda = 0.1$, $m_\Phi = 100$ GeV for spin-0 mediator (left-panel) and $\zeta = g_V$, $m_{Z'} = 100$ GeV for spin-1 mediator (right-panel). The green dashed line and black dashed line are constraints from XENON1T and PandaX-II experiments, respectively. The black solid line denotes the neutrino floor.

5 Summary

There are more than twenty DM direct detection experiments on the Earth searching for nuclear recoils induced by elastic WIMP-nucleon scattering and there are countless WIMP models on the market. Theoretically, which kind of WIMP deserves a deep investigation is a question worth pondering. It looks like to be a good strategy to study the direct detection signal of a WIMP model that has non-trivial signals in indirect detection experiments. The bottom quark flavored DM is one of well motivated models since it can interpret the cosmic ray antiproton excess observed by the AMS-02 Collaboration as well as the GeV-scale gamma ray excess observed from the Galactic center. In this paper, we have studied next-to-leading order corrections to the scattering cross section of the scalar-type bottom-quark-flavored DM with nucleon. We focused on two scenarios in which the direct detection cross sections are suppressed at the tree-level. Our results given in the Fig. 10 show that next-to-leading order corrections are sizable and it is possible to detect some parameter space of such models using current direct detection techniques. It should be mentioned that no matter the observed excesses in indirect detection experiments are induced by WIMP or not, a systematic study to the direct detection signal of a WIMP that might be detected in an indirect detection experiment is necessary as we do not know what kind of exotic signal will be brought to us in future observations.

Acknowledgments

This work was supported by the National Natural Science Foundation of China under grant No. 11775025 and the Fundamental Research Funds for the Central Universities under grant No. 2017NT17.

A Annihilation cross sections

Annihilation cross sections corresponding to spin-0 and spin-1 mediators are listed respectively as follows

- spin-0 mediator ($m_\varphi < m_\Phi$)

$$\begin{aligned} \sigma v = & \frac{f_P^2 \Lambda^2 \sqrt{m_\varphi^2 - m_b^2}}{4\pi m_\varphi ((m_\Phi^2 - 4m_\varphi^2)^2 + \Gamma_\Phi^2 m_\Phi^2)} \\ & + \frac{v^2 f_P^2 \Lambda^2}{32\pi m_\varphi \sqrt{m_\varphi^2 - m_b^2} ((m_\Phi^2 - 4m_\varphi^2)^2 + \Gamma_\Phi^2 m_\Phi^2)^2} \left[-2m_\varphi^2 m_\Phi^2 (\Gamma_\Phi^2 + m_\Phi^2 + 20m_b^2) \right. \\ & \left. + 16m_\varphi^4 (2m_\Phi^2 + 7m_b^2) - 96m_\varphi^6 + 3m_\Phi^2 m_b^2 (\Gamma_\Phi^2 + m_\Phi^2) \right] \end{aligned} \quad (\text{A.1})$$

- spin-0 mediator ($m_\varphi > m_\Phi$)

$$\begin{aligned} \sigma v = & \frac{\sqrt{m_\varphi^2 - m_\Phi^2}}{64\pi m_\varphi^3 (2m_\varphi^2 - m_\Phi^2)^2} (2\Lambda^2 - 2\lambda m_\varphi^2 + \lambda m_\Phi^2)^2 \\ & + \frac{v^2 (2\Lambda^2 - 2\lambda m_\varphi^2 + \lambda m_\Phi^2)}{1536\pi m_\varphi^3 \sqrt{m_\varphi^2 - m_\Phi^2} (2m_\varphi^2 - m_\Phi^2)^4} \left[3\lambda (4m_\varphi^2 - 5m_\Phi^2) (2m_\varphi^2 - m_\Phi^2)^3 \right. \\ & \left. + 2\Lambda^2 (148m_\varphi^4 m_\Phi^2 - 80m_\varphi^2 m_\Phi^4 - 80m_\varphi^6 + 15m_\Phi^6) \right] \end{aligned} \quad (\text{A.2})$$

- spin-1 mediator ($m_\varphi < m_{Z'}$)

$$\sigma v = \frac{v^2 \zeta^2 g_V^2 (2m_\varphi^2 + m_b^2)}{12\pi [(m_{Z'}^2 - 4m_\varphi^2)^2 + m_{Z'}^2 \Gamma_{Z'}^2]} \sqrt{1 - \frac{m_b^2}{m_\varphi^2}} \quad (\text{A.3})$$

- spin-1 mediator ($m_\varphi > m_{Z'}$)

$$\begin{aligned} \sigma v = & \frac{g_V^4 \sqrt{1 - m_{Z'}^2/m_\varphi^2}}{16\pi m_\varphi^2 (2m_\varphi^2 - m_{Z'}^2)^2} (-8m_\varphi^2 m_{Z'}^2 + 8m_\varphi^4 + 3m_{Z'}^4) \\ & + \frac{v^2 g_V^4}{384\pi m_\varphi^4 \sqrt{1 - m_{Z'}^2/m_\varphi^2} (2m_\varphi^2 - m_{Z'}^2)^4} \left(1888m_\varphi^8 m_{Z'}^2 - 2224m_\varphi^6 m_{Z'}^4 \right. \\ & \left. + 1332m_\varphi^4 m_{Z'}^6 - 392m_\varphi^2 m_{Z'}^8 - 640m_\varphi^{10} + 45m_{Z'}^{10} \right) \end{aligned} \quad (\text{A.4})$$

B Loop functions

Loop functions used in this work are collected as follows [56, 57]:

$$\int \frac{d^4 k}{(2\pi)^4} \frac{1}{[(p+k)^2 - m_\varphi^2][k^2 - m_a^2]} = \frac{i}{16\pi^2} B_0(p^2, m_a^2, m_\varphi^2) \quad (\text{B.1})$$

$$\int \frac{d^4 k}{(2\pi)^4} \frac{1}{[(p+k)^2 - m_\varphi^2][k^2 - m_a^2]^2} = \frac{i}{16\pi^2} C_0(p^2, m_a^2, m_\varphi^2) \quad (\text{B.2})$$

$$\int \frac{d^4 k}{(2\pi)^4} \frac{1}{[(p+k)^2 - m_\varphi^2][k^2 - m_a^2]^3} = \frac{i}{16\pi^2} D_0(p^2, m_a^2, m_\varphi^2) \quad (\text{B.3})$$

$$\int \frac{d^4 k}{(2\pi)^4} \frac{k^\mu}{[(p+k)^2 - m_\varphi^2][k^2 - m_a^2]^2} = \frac{i}{16\pi^2} p^\mu C_2(p^2, m_a^2, m_\varphi^2) \quad (\text{B.4})$$

$$\int \frac{d^4 k}{(2\pi)^4} \frac{1}{[(p+k)^2 - m_\varphi^2][k^2 - m_a^2][k^2 - m_Q^2]^n} = \frac{i}{16\pi^2} X_n(p^2, m_\varphi^2, m_a^2, m_Q^2) \quad (\text{B.5})$$

$$\int \frac{d^4 k}{(2\pi)^4} \frac{k^\mu}{[(p+k)^2 - m_\varphi^2][k^2 - m_a^2][k^2 - m_Q^2]^n} = \frac{i}{16\pi^2} p^\mu Y_n(p^2, m_\varphi^2, m_a^2, m_Q^2) \quad (\text{B.6})$$

$$\begin{aligned} \int \frac{d^4 k}{(2\pi)^4} \frac{k^\mu k^\nu}{[(p+k)^2 - m_\varphi^2]k^4[k^2 - m_a^2]^2} &= \frac{i}{16\pi^2} [p^\mu p^\nu Z_{11}(p^2, m_\varphi^2, m_a^2) \\ &\quad + g^{\mu\nu} Z_{00}(p^2, m_\varphi^2, m_a^2)] \end{aligned} \quad (\text{B.7})$$

The expressions for $\partial F_1(m_a^2)/\partial(m_a^2)$ and $\partial F_2(m_a^2)/\partial(m_a^2)$ using the loop functions are

$$\begin{aligned} \frac{\partial}{\partial m_a^2} F_1(m_a^2) &= \int_0^1 dx \left\{ 3 \frac{\partial}{\partial m_a^2} X_1(m_\varphi^2, m_\varphi^2, m_a^2, \frac{m_Q^2}{x(1-x)}) \right. \\ &\quad - m_Q^2 \frac{(2+5x-5x^2)}{x^2(1-x)^2} \frac{\partial}{\partial m_a^2} X_2(m_\varphi^2, m_\varphi^2, m_a^2, \frac{m_Q^2}{x(1-x)}) \\ &\quad \left. - 2m_Q^4 \frac{(1-2x+2x^2)}{x^3(1-x)^3} \frac{\partial}{\partial m_a^2} X_3(m_\varphi^2, m_\varphi^2, m_a^2, \frac{m_Q^2}{x(1-x)}) \right\} \end{aligned} \quad (\text{B.8})$$

$$\begin{aligned} \frac{\partial}{\partial m_a^2} F_2(m_a^2) &= \int_0^1 dx \left\{ 3 \frac{\partial}{\partial m_a^2} B_0(0, \frac{m_Q^2}{x(1-x)}, m_a^2) \right. \\ &\quad - m_Q^2 \frac{(2+5x-5x^2)}{x^2(1-x)^2} \frac{\partial}{\partial m_a^2} C_0(0, \frac{m_Q^2}{x(1-x)}, m_a^2) \\ &\quad \left. - 2m_Q^4 \frac{(1-2x+2x^2)}{x^3(1-x)^3} \frac{\partial}{\partial m_a^2} D_0(0, \frac{m_Q^2}{x(1-x)}, m_a^2) \right\} \end{aligned} \quad (\text{B.9})$$

All of these functions can be evaluated by using Package-X [68, 69]. For example, we give the analytical expression for $C_0(p^2, m_a^2, m_\varphi^2)$,

$$\begin{aligned} C_0(p^2, m_a^2, m_\varphi^2) &= \frac{1}{2p^2} \log \left(\frac{m_\varphi^2}{m_a^2} \right) - \left[\frac{(m_\varphi^2 - m_a^2 + p^2)}{p^2 \sqrt{m_a^4 - 2m_a^2 m_\varphi^2 - 2m_a^2 p^2 + m_\varphi^4 - 2m_\varphi^2 p^2 + p^4}} \right. \\ &\quad \left. \times \log \left(\frac{m_a^2 + m_\varphi^2 - p^2 + \sqrt{m_a^4 - 2m_a^2 m_\varphi^2 - 2m_a^2 p^2 + m_\varphi^4 - 2m_\varphi^2 p^2 + p^4}}{2m_a m_\varphi} \right) \right] \end{aligned} \quad (\text{B.10})$$

and the remaining functions can be evaluated in the same way.

C Nucleon form factors

We here give the definition of the nuclear form factors required to calculate the effective interactions between DM and nucleons. For the spin-independent interactions, we need the following nuclear form factors [4, 52]:

$$\langle N | m_q \bar{q} q | N \rangle = m_N f_{T_q}^N, \quad (q = u, d, s) \quad (\text{C.1})$$

$$\langle N | -\frac{9\alpha_s}{8\pi} G_{\mu\nu}^a G^{a\mu\nu} | N \rangle = m_N f_{T_G}^N, \quad (\text{C.2})$$

$$\langle N | \mathcal{O}_{\mu\nu}^q | N \rangle = \frac{1}{m_N} (p_\mu^N p_\nu^N - \frac{1}{4} m_N^2 g_{\mu\nu}) (q^N(2) + \bar{q}^N(2)) \quad (\text{C.3})$$

where m_N is the nucleon mass, $f_{T_q}^N$ and $f_{T_G}^N$ are nuclear form factors, q^N and \bar{q}^N are the second moments of the quark parton distribution functions and p_μ^N is the nucleon four-momentum. The present numerical values of the form factors for light quarks are taken from micrOMEGAs [70, 71]

$$\begin{aligned} f_{T_u}^p &= 0.01513, & f_{T_d}^p &= 0.0191, & f_{T_s}^p &= 0.0447, \\ f_{T_u}^n &= 0.0110, & f_{T_d}^n &= 0.0273, & f_{T_s}^n &= 0.0447, \end{aligned} \quad (\text{C.4})$$

which can be related to the gluon form factor via [4]

$$f_{T_G}^{p(n)} = 1 - \sum_{q=u,d,s} f_{T_q}^{p(n)}. \quad (\text{C.5})$$

The second moments are calculated at the scale $\mu = m_Z$ by using CTEQ parton distribution functions [31, 72]

$$\begin{aligned} g^p(2) &= 0.464, \\ u^p(2) &= 0.22, & \bar{u}^p(2) &= 0.034, \\ d^p(2) &= 0.11, & \bar{d}^p(2) &= 0.036, \\ s^p(2) &= 0.026, & \bar{s}^p(2) &= 0.026, \\ c^p(2) &= 0.019, & \bar{c}^p(2) &= 0.019, \\ b^p(2) &= 0.012, & \bar{b}^p(2) &= 0.012, \end{aligned} \quad (\text{C.6})$$

where the corresponding values for neutron can be obtained by interchanging up and down quarks.

References

- [1] PLANCK collaboration, *Planck 2018 results. VI. Cosmological parameters*, *Astron. Astrophys.* **641** (2020) A6 [[1807.06209](#)].
- [2] H. Goldberg, *Constraint on the Photino Mass from Cosmology*, *Phys. Rev. Lett.* **50** (1983) 1419.

- [3] J.R. Ellis, J.S. Hagelin, D.V. Nanopoulos, K.A. Olive and M. Srednicki, *Supersymmetric Relics from the Big Bang*, *Nucl. Phys.* **B238** (1984) 453.
- [4] G. Jungman, M. Kamionkowski and K. Griest, *Supersymmetric dark matter*, *Phys. Rept.* **267** (1996) 195 [[hep-ph/9506380](#)].
- [5] G. Servant and T.M.P. Tait, *Is the lightest Kaluza-Klein particle a viable dark matter candidate?*, *Nucl. Phys.* **B650** (2003) 391 [[hep-ph/0206071](#)].
- [6] H.-C. Cheng, J.L. Feng and K.T. Matchev, *Kaluza-Klein dark matter*, *Phys. Rev. Lett.* **89** (2002) 211301 [[hep-ph/0207125](#)].
- [7] G. Bertone, D. Hooper and J. Silk, *Particle dark matter: Evidence, candidates and constraints*, *Phys. Rept.* **405** (2005) 279 [[hep-ph/0404175](#)].
- [8] T. Lin, *Dark matter models and direct detection*, *PoS* **333** (2019) 009 [[1904.07915](#)].
- [9] T.R. Slatyer, *Indirect Detection of Dark Matter*, in *Proceedings, Theoretical Advanced Study Institute in Elementary Particle Physics : Anticipating the Next Discoveries in Particle Physics (TASI 2016): Boulder, CO, USA, June 6-July 1, 2016*, pp. 297–353, 2018, DOI [[1710.05137](#)].
- [10] D. Hooper, *TASI Lectures on Indirect Searches For Dark Matter*, *PoS TASI2018* (2019) 010 [[1812.02029](#)].
- [11] AMS collaboration, *Antiproton Flux, Antiproton-to-Proton Flux Ratio, and Properties of Elementary Particle Fluxes in Primary Cosmic Rays Measured with the Alpha Magnetic Spectrometer on the International Space Station*, *Phys. Rev. Lett.* **117** (2016) 091103.
- [12] I. Cholis, T. Linden and D. Hooper, *A Robust Excess in the Cosmic-Ray Antiproton Spectrum: Implications for Annihilating Dark Matter*, *Phys. Rev.* **D99** (2019) 103026 [[1903.02549](#)].
- [13] L. Goodenough and D. Hooper, *Possible Evidence For Dark Matter Annihilation In The Inner Milky Way From The Fermi Gamma Ray Space Telescope*, [0910.2998](#).
- [14] D. Hooper and L. Goodenough, *Dark Matter Annihilation in The Galactic Center As Seen by the Fermi Gamma Ray Space Telescope*, *Phys. Lett.* **B697** (2011) 412 [[1010.2752](#)].
- [15] D. Hooper and T. Linden, *On The Origin Of The Gamma Rays From The Galactic Center*, *Phys. Rev.* **D84** (2011) 123005 [[1110.0006](#)].
- [16] K.N. Abazajian and M. Kaplinghat, *Detection of a Gamma-Ray Source in the Galactic Center Consistent with Extended Emission from Dark Matter Annihilation and Concentrated Astrophysical Emission*, *Phys. Rev.* **D86** (2012) 083511 [[1207.6047](#)].
- [17] T. Daylan, D.P. Finkbeiner, D. Hooper, T. Linden, S.K.N. Portillo, N.L. Rodd et al., *The characterization of the gamma-ray signal from the central Milky Way: A case for annihilating dark matter*, *Phys. Dark Univ.* **12** (2016) 1 [[1402.6703](#)].
- [18] D. Hooper, R.K. Leane, Y.-D. Tsai, S. Wegsman and S.J. Witte, *A systematic study of hidden sector dark matter: application to the gamma-ray and antiproton excesses*, *JHEP* **07** (2020) 163 [[1912.08821](#)].
- [19] A. Berlin, D. Hooper and S.D. McDermott, *Simplified Dark Matter Models for the Galactic Center Gamma-Ray Excess*, *Phys. Rev.* **D89** (2014) 115022 [[1404.0022](#)].
- [20] U. Haisch and F. Kahlhoefer, *On the importance of loop-induced spin-independent interactions for dark matter direct detection*, *JCAP* **1304** (2013) 050 [[1302.4454](#)].

- [21] A. Crivellin and U. Haisch, *Dark matter direct detection constraints from gauge bosons loops*, *Phys. Rev.* **D90** (2014) 115011 [[1408.5046](#)].
- [22] F. D’Eramo, B.J. Kavanagh and P. Panci, *You can hide but you have to run: direct detection with vector mediators*, *JHEP* **08** (2016) 111 [[1605.04917](#)].
- [23] A. Crivellin, F. D’Eramo and M. Procura, *New Constraints on Dark Matter Effective Theories from Standard Model Loops*, *Phys. Rev. Lett.* **112** (2014) 191304 [[1402.1173](#)].
- [24] F. Bishara, J. Brod, B. Grinstein and J. Zupan, *Renormalization Group Effects in Dark Matter Interactions*, *JHEP* **03** (2020) 089 [[1809.03506](#)].
- [25] T. Li, *Revisiting the direct detection of dark matter in simplified models*, *Phys. Lett.* **B782** (2018) 497 [[1804.02120](#)].
- [26] N.F. Bell, G. Busoni and I.W. Sanderson, *Loop Effects in Direct Detection*, *JCAP* **1808** (2018) 017 [[1803.01574](#)].
- [27] J. Hisano, K. Ishiwata and N. Nagata, *A complete calculation for direct detection of Wino dark matter*, *Phys. Lett.* **B690** (2010) 311 [[1004.4090](#)].
- [28] J. Hisano, K. Ishiwata, N. Nagata and T. Takesako, *Direct Detection of Electroweak-Interacting Dark Matter*, *JHEP* **07** (2011) 005 [[1104.0228](#)].
- [29] F. Ertas and F. Kahlhoefer, *Loop-induced direct detection signatures from CP-violating scalar mediators*, *JHEP* **06** (2019) 052 [[1902.11070](#)].
- [30] K. Ishiwata and T. Toma, *Probing pseudo Nambu-Goldstone boson dark matter at loop level*, *JHEP* **12** (2018) 089 [[1810.08139](#)].
- [31] T. Abe, M. Fujiwara and J. Hisano, *Loop corrections to dark matter direct detection in a pseudoscalar mediator dark matter model*, *JHEP* **02** (2019) 028 [[1810.01039](#)].
- [32] W. Chao, G.-J. Ding, X.-G. He and M. Ramsey-Musolf, *Scalar Electroweak Multiplet Dark Matter*, *JHEP* **08** (2019) 058 [[1812.07829](#)].
- [33] K. Ghorbani and P.H. Ghorbani, *Leading Loop Effects in Pseudoscalar-Higgs Portal Dark Matter*, *JHEP* **05** (2019) 096 [[1812.04092](#)].
- [34] T. Li and P. Wu, *Simplified dark matter models with loop effects in direct detection and the constraints from indirect detection and collider search*, *Chin. Phys.* **C43** (2019) 113102 [[1904.03407](#)].
- [35] W. Chao, *Direct detections of Majorana dark matter in vector portal*, *JHEP* **11** (2019) 013 [[1904.09785](#)].
- [36] J. Monroe and P. Fisher, *Neutrino Backgrounds to Dark Matter Searches*, *Phys. Rev.* **D76** (2007) 033007 [[0706.3019](#)].
- [37] L.E. Strigari, *Neutrino Coherent Scattering Rates at Direct Dark Matter Detectors*, *New J. Phys.* **11** (2009) 105011 [[0903.3630](#)].
- [38] J. Billard, L. Strigari and E. Figueroa-Feliciano, *Implication of neutrino backgrounds on the reach of next generation dark matter direct detection experiments*, *Phys. Rev.* **D89** (2014) 023524 [[1307.5458](#)].
- [39] G.B. Gelmini, V. Takhistov and S.J. Witte, *Casting a Wide Signal Net with Future Direct Dark Matter Detection Experiments*, *JCAP* **1807** (2018) 009 [[1804.01638](#)].

- [40] C. Boehm, D.G. Cerdeno, P.A.N. Machado, A. Olivares-Del Campo, E. Perdomo and E. Reid, *How high is the neutrino floor?*, *JCAP* **1901** (2019) 043 [[1809.06385](#)].
- [41] W. Chao, J.-G. Jiang, X. Wang and X.-Y. Zhang, *Direct Detections of Dark Matter in the Presence of Non-standard Neutrino Interactions*, *JCAP* **1908** (2019) 010 [[1904.11214](#)].
- [42] J. Hisano, R. Nagai and N. Nagata, *Effective Theories for Dark Matter Nucleon Scattering*, *JHEP* **05** (2015) 037 [[1502.02244](#)].
- [43] J. Hisano, *Effective theory approach to direct detection of dark matter*, in *Proceedings, Les Houches summer school: EFT in Particle Physics and Cosmology: Les Houches (Chamonix Valley), France*, vol. 108, 2020, DOI [[1712.02947](#)].
- [44] J. Hisano, K. Ishiwata and N. Nagata, *Gluon contribution to the dark matter direct detection*, *Phys. Rev.* **D82** (2010) 115007 [[1007.2601](#)].
- [45] J. Hisano, K. Ishiwata and N. Nagata, *QCD Effects on Direct Detection of Wino Dark Matter*, *JHEP* **06** (2015) 097 [[1504.00915](#)].
- [46] P. Gondolo and G. Gelmini, *Cosmic abundances of stable particles: improved analysis.*, *Nuclear Physics B* **360** (1991) 145.
- [47] J. Ellis, *TikZ-Feynman: Feynman diagrams with TikZ*, *Comput. Phys. Commun.* **210** (2017) 103 [[1601.05437](#)].
- [48] J. Lewin and P. Smith, *Review of mathematics, numerical factors, and corrections for dark matter experiments based on elastic nuclear recoil*, *Astropart. Phys.* **6** (1996) 87.
- [49] R.H. Helm, *Inelastic and Elastic Scattering of 187-Mev Electrons from Selected Even-Even Nuclei*, *Phys. Rev.* **104** (1956) 1466.
- [50] J. Read, *The Local Dark Matter Density*, *J. Phys. G* **41** (2014) 063101 [[1404.1938](#)].
- [51] V. Barger, W.-Y. Keung and D. Marfatia, *Electromagnetic properties of dark matter: Dipole moments and charge form factor*, *Phys. Lett. B* **696** (2011) 74 [[1007.4345](#)].
- [52] M.A. Shifman, A. Vainshtein and V.I. Zakharov, *Remarks on Higgs Boson Interactions with Nucleons*, *Phys. Lett. B* **78** (1978) 443.
- [53] J.R. Ellis, K.A. Olive and C. Savage, *Hadronic Uncertainties in the Elastic Scattering of Supersymmetric Dark Matter*, *Phys. Rev.* **D77** (2008) 065026 [[0801.3656](#)].
- [54] V. Novikov, M.A. Shifman, A. Vainshtein and V.I. Zakharov, *Calculations in External Fields in Quantum Chromodynamics. Technical Review*, *Fortsch. Phys.* **32** (1984) 585.
- [55] V. Shtabovenko, R. Mertig and F. Orellana, *New Developments in FeynCalc 9.0*, *Comput. Phys. Commun.* **207** (2016) 432 [[1601.01167](#)].
- [56] G. Passarino and M. Veltman, *One Loop Corrections for $e^+ e^-$ Annihilation Into $\mu^+ \mu^-$ in the Weinberg Model*, *Nucl. Phys. B* **160** (1979) 151.
- [57] T. Abe and R. Sato, *Quantum corrections to the spin-independent cross section of the inert doublet dark matter*, *JHEP* **03** (2015) 109 [[1501.04161](#)].
- [58] K.G. Chetyrkin, B.A. Kniehl and M. Steinhauser, *Decoupling relations to $O(\alpha_s^3)$ and their connection to low-energy theorems*, *Nucl. Phys.* **B510** (1998) 61 [[hep-ph/9708255](#)].
- [59] D.J. Gross and F. Wilczek, *ASYMPTOTICALLY FREE GAUGE THEORIES. 2.*, *Phys. Rev.* **D9** (1974) 980.

- [60] L. Lopez Honorez, E. Nezri, J.F. Oliver and M.H.G. Tytgat, *The Inert Doublet Model: An Archetype for Dark Matter*, *JCAP* **0702** (2007) 028 [[hep-ph/0612275](#)].
- [61] V. Barger, P. Langacker, M. McCaskey, M.J. Ramsey-Musolf and G. Shaughnessy, *LHC Phenomenology of an Extended Standard Model with a Real Scalar Singlet*, *Phys. Rev.* **D77** (2008) 035005 [[0706.4311](#)].
- [62] R.N. Mohapatra and R.E. Marshak, *Local B-L Symmetry of Electroweak Interactions, Majorana Neutrinos and Neutron Oscillations*, *Phys. Rev. Lett.* **44** (1980) 1316.
- [63] W. Chao, H.-k. Guo and Y. Zhang, *Majorana Dark matter with B+L gauge symmetry*, *JHEP* **04** (2017) 034 [[1604.01771](#)].
- [64] X.-G. He, G.C. Joshi, H. Lew and R.R. Volkas, *Simplest Z-prime model*, *Phys. Rev.* **D44** (1991) 2118.
- [65] J. Edsjo and P. Gondolo, *Neutralino relic density including coannihilations*, *Phys. Rev.* **D56** (1997) 1879 [[hep-ph/9704361](#)].
- [66] XENON collaboration, *First Dark Matter Search Results from the XENON1T Experiment*, *Phys. Rev. Lett.* **119** (2017) 181301 [[1705.06655](#)].
- [67] PANDAX-II collaboration, *Dark Matter Results from First 98.7 Days of Data from the PandaX-II Experiment*, *Phys. Rev. Lett.* **117** (2016) 121303 [[1607.07400](#)].
- [68] H.H. Patel, *Package-X: A Mathematica package for the analytic calculation of one-loop integrals*, *Comput. Phys. Commun.* **197** (2015) 276 [[1503.01469](#)].
- [69] H.H. Patel, *Package-X 2.0: A Mathematica package for the analytic calculation of one-loop integrals*, *Comput. Phys. Commun.* **218** (2017) 66 [[1612.00009](#)].
- [70] G. Belanger, F. Boudjema, A. Pukhov and A. Semenov, *Dark matter direct detection rate in a generic model with micrOMEGAs 2.2*, *Comput. Phys. Commun.* **180** (2009) 747 [[0803.2360](#)].
- [71] G. Bélanger, F. Boudjema, A. Goudelis, A. Pukhov and B. Zaldivar, *micrOMEGAs5.0 : Freeze-in*, *Comput. Phys. Commun.* **231** (2018) 173 [[1801.03509](#)].
- [72] J. Pumplin, D. Stump, J. Huston, H. Lai, P.M. Nadolsky and W. Tung, *New generation of parton distributions with uncertainties from global QCD analysis*, *JHEP* **07** (2002) 012 [[hep-ph/0201195](#)].